Topics in Catalysis (2013) 56:1033-1046.
DOI 10.1007/s11244-013-0067-5

Controlled synthesis of Pt_3Sn/C electrocatalysts with exclusive Sn-Pt interaction designed for use in direct methanol fuel cells

Irina Borbáth[1], Dorottya Gubán[1], Zoltán Pászti[1], István E. Sajó[1], Eszter Drotár[1], José Luis Gómez de la Fuente[2], Tirma Herranz[2], Sergio Rojas[2] and András Tompos[1] (corresponding author)

[1]*Institute of Materials and Environmental Chemistry, Research Centre for Natural Sciences, HAS; POB 17, 1525 Budapest, Hungary*
e-mail: tompos.andras@ttk.mta.hu

[2]*Grupo de Energía y Química Sostenible; Instituto de Catálisis y Petroleoquímica, CSIC. C/Marie Curie 2, 28049, Madrid, Spain*

Published online: 16 May 2013

Abstract Alloy-type Sn-Pt/C electrocatalysts with Pt/Sn= 1.8-3.0 ratios and exclusive Sn-Pt interaction have been prepared by means of Controlled Surface Reactions (CSRs). As demonstrated by XRD the incorporation of Sn onto Pt/C was achieved satisfactorily yielding a near-stoichiometric fcc Pt_3Sn alloy phase along with a certain amount of the $Pt_{(1-x)}Sn_x$ solid solution. The content and dispersion of the fcc Pt_3Sn phase within the electrocatalysts can be controlled by tuning the reaction conditions of CSRs. No evidence of the presence of SnO_2 phases in the Sn-modified Pt/C samples were found by means of the XRD and EDS analysis. According to in situ XPS studies the pre-treatment in hydrogen at 350°C resulted in complete reduction of tin to Sn^0. These results demonstrate that the method of CSRs is a powerful tool to create of Pt-Sn bimetallic nanoparticles exclusively, without tin introduction onto the carbon support. The performance of the intermetallic SnPt/C catalysts in the CO and methanol electrooxidation reactions depends on the actual composition of the exposed surface and the size of bimetallic particles. In the consecutive tin introduction the decrease of the amount of $SnEt_4$ precursor added per period, accompanied with an increase of the number of anchoring periods, resulted in an increase of the activity in both electrooxidation reactions as a consequence of an optimal balance of Pt/Sn ratio, the content of fcc Pt_3Sn phase and metal particle size. It was demonstrated that the increasing tin content above a certain (optimal) amount gives rise to a negative effect on the catalyst performance in the CO and methanol electrooxidation.

Keywords PtSn/C electrocatalysts, Controlled Surface Reactions, Pt_3Sn, Anode catalyst, electrooxidation

1 Introduction

According generally accepted pathways CO is supposed to be one of the intermediates of electrooxidation of different alcohols. Therefore, high tolerance to CO is one of the criteria for the preparation of efficient alcohol electrooxidation catalysts. Platinum is commonly used as anode catalyst in direct alcohol fuel cells. However, pure Pt is not the most efficient anodic catalyst, being rapidly poisoned by strongly adsorbed species [1,2]. To enhance the electrooxidation ability of Pt/C, *i.e.*, to shift the onset potential for the electrooxidation of CO and C_1-C_2 alcohols to less positive values, they are usually modified with oxophilic metals such as Ru, Mo, Ni or Sn [2-8]. Among them, Sn-modified Pt/C electrocatalysts are recognized as the most active electrodes [9,10].

SnPt/C electrocatalysts can be prepared by means of versatile techniques. Most synthetic routes lead to solids with a wide range of phases such as Pt, either reduced or oxide, Sn oxides and Pt-Sn alloys or $Pt_{(1-x)}Sn_x$ solid solutions with different stoichiometry [1,10,11]. It has been demonstrated [11] that Pt-Sn alloys are one of the most active bimetallic systems. There is also a widespread consensus that the Pt_3Sn phase is the most active one in electrooxidation of CO [9,11,12]. In analyzing various reports, it seems that production of Pt_3Sn alloy as a pure and exclusive phase rarely occurs and its presence strongly depends on the synthetic procedure [1,2,13].

SnPt/C catalysts are usually prepared by impregnation [8] and water-in-oil microemulsion methods [14-16], followed by high-temperature treatment. The main disadvantage of these methods is the quite unlikely formation of bimetallic particles. In the preparation of the desired well-dispersed Pt_3Sn intermetallic phase by the impregnation-reduction approach the importance of the elimination of chloride ions prior to any thermal treatments was emphasized in Refs. [10,17].

The preparation of Sn-modified Pt/C catalysts using the well-known “Bönnemann” method has been studied extensively [18,19]. Depending on the reaction conditions, the mixture of $Pt_{0.81}Sn_{0.19}$ and hcp PtSn alloy phases [20] or fully non-alloyed Pt/SnO_2 nanoparticles [13] can be obtained.

The polyol synthesis has recently been extended to produce SnPt/C catalysts [21-23]. The presence of tin in different forms (Pt-Sn alloys versus fully non-alloyed Pt/SnO_x particles) has been achieved by modified polyol methods [24-26]. Low activities of the polyol type catalysts in the ethanol oxidation reaction [27] have been ascribed to the low degree of Pt-Sn alloy formation. Highly dispersed and partially alloyed SnPt/C catalysts can also be prepared by a microwave-assisted polyol process [28] and the borohydride reduction method [29]. The best

performance in a direct methanol fuel cells was obtained using the Pt_3Sn/C alloy catalysts prepared by the treatment with formic acid [1,30] because of an optimal balance of Sn content, degree of alloying and metal particle size [31].

Upon using the polymeric precursor method (PPM) [32] the absence of metallic Sn and the presence of pure fcc Pt and the SnO_2 phases in SnPt/C catalysts has been demonstrated in Ref. [33]. However, the formation of Pt_3Sn alloy phase was recently achieved by a modified PPM [34]. Controlled formation of Pt-Sn alloy nanoparticles with cubic and hexagonal structure can been done by the "heating up" method [35].

Exclusive formation of supported Pt-Sn alloy phases with different Pt/Sn ratios can also be achieved by using anchoring type Controlled Surface Reactions (CSRs) between hydrogen adsorbed on Pt sites and tetraalkyl tin compounds (SnR_4) [36-38]. The surface chemistry involved can be written as follows [36]:

$$PtH_{ads} + SnR_4 \rightarrow Pt\text{-}SnR_{(4-x)} + x\ RH \quad (1)$$

$$Pt\text{-}SnR_{(4-x)} + (4-x)/2\ H_2 \rightarrow Pt\text{-}Sn + (4-x)\ RH \quad (2)$$

The use of the above a two step approach gives a definite guaranty for the exclusive introduction of tin onto platinum, *i.e.* for the suppression of Sn-support interaction. In the frame of our previous studies the modes and ways to increase the amount of tin introduced directly onto the parent metal has been established [36,39]. The use of extremely high concentration of SnR_4 should be avoided as it results in a concentration gradient of the anchored modifier. It has been demonstrated that the use of the consecutive reactions can decrease the inhomogeneity of the modifier over the metal particles [40].

In our recent studies [9,41] upon use of CSRs a series of SnPt/C catalysts highly active in CO and C_1-C_2 alcohols electrooxidation reactions have been prepared. Upon using reaction temperature T_r= 70-120^{o}C, different number of consecutive tin anchoring periods and atmospheric H_2 pressure SnPt/C catalysts with relatively low tin content (Pt/Sn > 3) was obtained [9]. This synthetic route results in the exclusive incorporation of Sn onto the Pt sites. A clear correlation between Pt_3Sn content and the electrocatalytic performance has also been established. The decrease of $E_{CO,onset}$ from 620 to 210 mV and $E_{EtOH,\ onset}$ from 310 to 100 mV has been observed on the Pt/C and SnPt/C catalyst (Pt/Sn= 4), respectively.

In our recent study [41] reaction conditions of CSRs has been tuned (T_r= 170^{o}C, p_{H2}= 5 bar) in order to achieve higher loading of Sn over Pt/C catalyst (Pt/Sn= 0.8 and 1.7) within significantly shorter reaction time. It has been proved [41] that the performance of Pt_3Sn (fcc)

phase is superior to that of the PtSn (hcp) phase for both CO and methanol oxidation reactions (MOR).

It is necessary to mention that tetra-*n*-butyltin has also been applied to prepare SnPt/C catalysts for fuel cell application [42], however in that study no attempt was done to control the exclusive formation of bimetallic entities.

This work describes a modification of the CSRs for the preparation of alloy-type SnPt/C electrocatalysts with the desired Pt/Sn= 3 ratio and homogeneous tin distribution over the Pt nanoparticles. Efforts were made to adjust synthesis parameters with the aim to get carbon supported fcc Pt_3Sn alloy phase in high extent (or even exclusively). As CO is supposed to be an intermediate in methanol electrooxidation the Pt_3Sn alloy might facilitate methanol electrooxidation reaction as well. The goal was to study the influence of experimental conditions, mainly the initial concentration of $SnEt_4$ and the number of the consecutive tin anchoring periods, on i) the actual composition of formed bimetallic phases, ii) chemical state of Sn and Pt, and iii) presence or absence of both unmodified Pt and SnO_x phases. The performance of these catalysts has been evaluated in both electrooxidation reactions.

2 Experimental section

2.1 Synthesis of Sn modified Pt/C catalysts

40 wt.% commercial Pt/C catalysts (Quintech) was modified with tetraethyltin ($SnEt_4$) in order to obtain SnPt/C catalysts with Pt/Sn=1.8-3.0 ratios. The $SnEt_4$ and solvents (*n*-decane and *n*-hexane) were used as received (Sigma-Aldrich).

A 40 ml stainless steel autoclave with Pyrex glass lining was used. 200 mg of the Pt/C catalyst was suspended in 10 ml *n*-decane. The autoclave was purged with H_2 for 10 minutes and then the hydrogen pressure was set up to 5 bars. The reactor was immersed in an oil bath and heated up to 170°C. Then under vigorous stirring the tin anchoring step I (see reaction (1)) was started by an addition of the first amount of $SnEt_4$ dissolved in *n*-decane. For this purpose the requested amount of $SnEt_4$ (needed for the preparation of SnPt/C catalysts with desired Pt/Sn ratio) was divided into several uniform portions and introduced into the reactor after equal periods of time. As duration of one anchoring period was 1 h. After 1 h the next portion of the appropriate *n*-decane solution of $SnEt_4$ was added. Preparation details and chemical composition of catalysts are listed in Table 1. Denomination of the different SnPt/C samples indicates main parameters of the synthesis. Accordingly, the first number shows the tin content in weight percent, whereas the roman numbers reflect the number of tin anchoring

periods. Sample A and B differ from each other in the initial [$SnEt_4$] concentration added per one tin anchoring period.

After the modification procedure, the catalyst was separated by centrifugation and carefully washed twice with 20 ml *n*-decane and tree times with 20 ml *n*-hexane. The catalyst was dried in air at 60°C for 1 h.

Before and after the modification procedure the [$SnEt_4$] concentration in *n*-decane was analyzed using the ν_{Sn-C} stretching band at 507 cm^{-1} (spectrum not shown) by Nicolet Avatar 320 FT-IR spectrometer [41]. The tin content and Pt/Sn ratios presented in Table 1 were calculated from these results.

After the surface modification the catalysts were treated in H_2 atmosphere by Temperature Programmed Reduction (TPR) technique (step II) using the following experimental parameters: heating interval= 25-350°C, heating rate= 5°C/min, H_2 flow rate= 30 ml/min. In some cases the final temperature of H_2 pre-treatment (T_{red}) was 250 or 400°C (details see in Table 2). Catalysts were kept at final temperature for 2 h then the furnace was cooled down in flowing H_2 to 50°C. The atmosphere was changed to nitrogen and the system was cooled down to room temperature under flowing nitrogen.

In order to make sure that the tetraethyltin compound does not react with the bare carbon support a blank experiment was done. The experiment performed at T_r= 170°C and P_{H2}= 5 bar with 0.03 M [$SnEt_4$] solution in *n*-decane shows that no reaction occurred between the organotin compound and the carbon support. The tin content was analyzed by ICP-OES. Good agreement between the tin content calculated by FT-IR spectroscopy and the amount of tin determined by ICP-OES was observed.

2.2 Physicochemical characterization

X-ray powder diffraction (XRD) patterns were obtained in a Philips model PW 3710 based PW 1050 Bragg-Brentano parafocusing goniometer using CuK_α radiation (λ= 0.15418 nm), graphite monochromator and proportional counter. Silicon powder (NIST SRM 640) was used as an internal standard and the scans were evaluated with profile fitting methods. The cell parameters of the crystalline phases were determined from the fitted d-values. Crystallite sizes were calculated from reflection line broadening using the Scherrer-equation.

Transmission Electron Microscopy (TEM) studies of the samples were made by use of a FEI Morgagni 268D type transmission electron microscope (accelerating voltage: 100 kV, W-filament). The samples were prepared by grinding and dispersing of the resulted powder in ethanol using an ultrasonic bath. TEM image of the blank Pt/C sample was also included. The

blank Pt/C sample underwent the same preparation procedure as the bimetallic catalysts but the solution of *n*-decane introduced contained no $SnEt_4$. This way the influence of the preparation procedure on the dispersion of the metallic particles of the parent Pt/C catalyst was studied. The average diameter was calculated by measuring the diameters of no less than 700 randomly selected metal particles from the non-aggregated areas in at least tree micrographs of each sample. Energy Dispersive X-ray Spectrometer (EDS) analysis was performed in an INCA (Oxford Instruments Ltd.) detector and an INCAEnergy software package. EDS analysis of individual particles was possible by using ZEISS EVO 40XVP Scanning Electron Microscope (accelerating voltage: 20kV, W-filament).

X-ray photoelectron spectroscopy (XPS) measurements were carried out using an EA125 electron spectrometer manufactured by OMICRON Nanotechnology GmbH (Germany). The photoelectrons were excited by MgKα (1253.6 eV) radiation. Spectra were recorded in the Constant Analyser Energy mode of the energy analyser with 30 eV pass energy resulting in a spectral resolution of 1 eV.

For XPS experiments two samples (8.3SnPt/C-III-A and 8.3SnPt/C-IV) in the form of fine powder were suspended in hexane. Drops of this suspension were placed on standard OMICRON sample plates; after evaporation of hexane catalyst coatings with sufficient adhesion and electric conductivity were obtained. First, both samples were analyzed in their "as received" state. Next, 8.3SnPt/C-III-A sample was also investigated after reduction in the high pressure cell of the spectrometer in 500 mbar H_2 at 350°C for 2 h (H_2 treated samples). In addition, this sample was also investigated after deliberate exposure to ambient air for a day (re-oxidized sample).

To this end, C 1s, O 1s, Pt 4f and Sn 3d core levels were analyzed; the most intense component of the C 1s envelope was set at 284.5 eV (graphite) and used as internal reference. Data were processed using the CasaXPS software package [43] by fitting the spectra with Gaussian-Lorentzian product peaks after removing a Shirley or linear background. Nominal surface compositions were calculated using the XPS MultiQuant software package [44,45], with the assumption of homogeneous depth distribution for all components. Chemical states were identified by XPS databases [46,47].

2.3 Electrochemical characterization

The bimetallic samples were investigated in details: both MOR and CO_{ad} stripping have been measured. The working electrode was a glassy carbon electrode (d= 0.3 cm, A= 0.0707 cm^2) that supported the catalyst. 1.3 μl from a suspension consisting of 5 mg of the catalysts,

0.500 ml of ethylene glycol, 0.2 ml of isopropanol and 30 μl Nafion has been dropped over the electrode surface and dried for 30 minutes. Ag/AgCl and Pt was used as reference and counter electrodes, respectively. The electrolyte applied was 0.5 M H_2SO_4. Cyclic voltammetry was used to clean and activate the catalysts. 100 cycles were performed at 1000 mV s^{-1} between -0.05 and 1.65 V (vs. NHE).

Electrochemical oxidation of methanol has been studied by means of cyclic voltammetry. The working electrode as well as the reference and counter electrodes were identical as described previously. The electrolyte contained 0.5 M H_2SO_4 and 1 M methanol. Cyclic voltammetry was done at 10 mV s^{-1} between 0.05 and 1.0 V (vs. NHE).

The amount of adsorbed CO (CO_{ad}) over the catalysts has been measured by CO stripping voltammetry in 0.5 M H_2SO_4. Gaseous CO was fed into the cell for 30 min while maintaining a constant voltage of 0.02 V (vs. NHE). After CO removal (nitrogen purge for 30 min), the working electrode was subjected to a cyclic voltammetry step at a 10 mV s^{-1} scan rate between 0.05 and 1.3 V (vs. NHE), and 3 consecutive cycles were recorded.

In situ electrochemical infrared reflection-adsorption spectroscopy (EC-IRAS) studies of the methanol and carbon monoxide oxidation reactions were performed with a NICOLET 6700 FT-IR spectrometer equipped with a MCT detector and fitted with a PIKE Technologies VeeMAX II spectroscopic accessory. A poly (methyl methacrylate) (PMMA) cell with a CaF_2 prism bevelled at 60º at its bottom was used. FTIR spectra were acquired from the average of 64 interferograms, obtained with 4 cm^{-1} resolution at selected potential, by applying single potential steps from a reference potential (E_0) in the positive direction up to 0.8 V. The reflectance ratio R/R_0 was calculated where R and R_0 are the reflectance measured at the sample and the reference potential, respectively. The reference potential R_0 was recorded at 0.05 V. Electrochemical control was carried out using an Autolab PGstat 302N.

3 Results and discussion

3.1 Preparation of Sn-Pt/C electrocatalysts

Experimental results related to tin anchoring onto the parent Pt/C catalyst are summarized in Table 1. It is known from our earlier studies [36,37,48] that upon using long reaction time, high reaction temperature and [$SnEt_4$] concentration the possibility of undesired reactions involving the anchoring groups of the support and the tin precursor compound can not be totally excluded. For this reason upon preparation of the catalysts with high tin content the key experimental variables (see Table 1) are as follows: (i) the number of consecutive tin anchoring periods and (ii) the amount of $SnEt_4$ introduced per one period.

As can be seen in Table 1, catalysts with desired Pt/Sn ratio ca. 3 was prepared upon using either low [$SnEt_4$] concentration connected with elevated number of tin anchoring periods (line 1 in Table 1) or higher [$SnEt_4$] concentration and lower number of anchoring period (lines 2 and 6 in Table 1). A systematic increase of Sn content was achieved by the increase of the number of the tin anchoring periods (compare lines 2-4 in Table 1). Upon use of increased [$SnEt_4$] concentration ([$SnEt_4$]= 0.034 M) and three tin anchoring periods the catalyst with intermediate Pt/Sn= 2.7 ratio (line 5 in Table 1) was obtained.

Table 1 Summary of results of 40 wt% Pt/C catalyst modification with $SnEt_4$

Samples	**V_{SnEt4},[a]**	**[$SnEt_4$],[b]**	**Number**	**[$SnEt_4$]$_0$,[c]**	**$SnEt_4$,[d]**	**Sn,[e]**	**Pt/Sn**
	ml	**M**	**of periods**	**mM**	**mmol**	**wt.%**	**at/at**
8.3SnPt/C-IV	1.5	0.023	4	3.04	0.140	8.3	2.9
8.3SnPt/C-III-A	1.5	0.031	3	4.03	0.139	8.3	3.0
11.0SnPt/C-IV	1.5	0.031	4	4.03	0.185	11.0	2.2
13.8SnPt/C-V	1.5	0.031	5	4.03	0.232	13.8	1.8
9.1SnPt/C-III	1.5	0.034	3	4.43	0.153	9.1	2.7
8.3SnPt/C-III-B	0.75	0.062	3	5.45 [f]	0.139	8.3	3.0

Amount of the Pt/C catalyst: 0.2 g, Pt content: 40 wt.%, solvent: *n*-decane (V_{C10H22}= 10 ml), reaction temperature: T_r= 170°C, atmosphere: H_2, hydrogen pressure: P_{H2}= 5 bar, duration of one tin anchoring period: 1 h

[a] Amount of *n*-decane solution of $SnEt_4$ added in one tin anchoring period

[b] Concentration of $SnEt_4$ solution in *n*-decane added per each period

[c] Initial concentration of $SnEt_4$ in the reaction mixture at the beginning of tin anchoring step I (period 1)

[d] Total amount of tin introduced during tin anchoring step I

[e] Tin content calculated from the results of FT-IR spectroscopy

[f] V_{C10H22}= 7.75 ml

In our previous study it has also been demonstrated [9] that upon using T_r= 70-120°C and atmospheric H_2 pressure during step I almost complete hydrogenolysis (~96 %) of anchored - $SnR_{(4-x)}$ surface species can be achieved. The maximum of very small TPR ethane peak (step II) was at around 140°C [9]. Based on this observation it can be proposed that in this work upon using extreme reaction conditions (T_r= 170°C, p_{H2}= 5 bar) the complete cleavage of the Sn-C σ-bonds and formation of "naked" tin (*x*= 4) over platinum during step I can be guaranteed. This form of tin can exist in a form of ad-atoms and/or migrate into the bulk of Pt and form alloy-type species. The conditions of high-temperature H_2 pre-treatment are summarized in Table 2.

It has also been known that catalysts supported on functionalized carbon could not tolerate high thermal treatment, due to the instability of surface oxygen groups of the support, which act as primary anchoring centres for metal precursors, facilitating the high dispersion of the metal phase [49-53].

In present study in order to increase the content of the desired fcc Pt_3Sn phase and to minimize the sintering of the metal nanoparticles an attempt was done to optimize the final temperature of H_2 pre-treatment (T_{red}) used in TPR experiments (step II).

Table 2 Average crystallite size and lattice parameter of the Sn modified Pt/C catalysts determined by XRD analysis

Samples	**Pt/Sn**	**T_{red}, °C[a]**	**Lattice parameter, Å (Phase, %)**			**Average crystallite size, nm**		
	at/at		**fcc $Pt_{1-x}Sn_x$ [b]**	**fcc Pt_3Sn [c]**	**hcp PtSn**	**$Pt_{1-x}Sn_x$**	**Pt_3Sn**	**PtSn**
8.3SnPt/C-IV	2.9	350	a: 3.933 (25%)	a: 3.975 (75%)	-	8.3	8.3	-
8.3SnPt/C-IIIB	3.0	350	a: 3.933 (28%)	a: 3.975 (72%)	-	9.1	9.1	-
8.3SnPt/C-IIIA	3.0	400	a: 3.94 (15%)	a: 3.99 (85%)	-	8.3	10.0	-
9.1SnPt/C-III	2.7	350	a: 3.933 (20%)	a: 3.985 (80%)	-	9.1	10.0	-
		250	a: 3.933 (25%)	a: 3.985 (75%)	-	6.6	7.7	-
		without TPR [d]	a: 3.933 (75%)	a: 3.985 (25%)	-	6.6	7.7	-
11.0SnPt/C-IV	2.2	350	a: 3.945 (35%)	a: 3.99 (60%)	(5%)	5.8	12.0	5.8
13.8SnPt/C-V	1.8	350	a: 3.945 (20%)	a: 3.99 (70%)	(10%)	9.1	17.0	14.0

[a] Duration of high-temperature H_2 pre-treatment: 2 h
[b] Pt lattice parameter = a: 3.917 Å
[c] fcc Pt_3Sn lattice parameter = a: 4.0015 Å
[d] Without high-temperature treatment in H_2

The influence of the T_{red} on the type of Sn-Pt alloys was demonstrated in Ref. [54]. It was shown that reduction of unsupported PtSn powder with a nominal Pt/Sn= 3 ratio at 200°C resulted in the formation of alloy phases with different tin content: Sn-rich alloy with surface character, and bulk Pt-rich alloy phase. Exclusive formation of Pt_3Sn alloy was observed only after reduction at 400°C.

Based on these observations the final reduction temperature used in step II was T_{red}= 250, 350 or 400°C (details see in Table 2).

3.2 Physicochemical characterization of Sn-Pt/C electrocatalysts

The results of different preparation procedures can be successfully characterized by XRD study. According to the XRD results the preparation condition favouring to the formation of the desired fcc Pt_3Sn phase can be chosen. In this way the preparation of SnPt/C catalysts can be controlled.

Typical X-ray diffraction pattern of Sn-Pt/C catalyst is shown in Fig. 1. Fig. 2A-D shows the influence of the preparation conditions on the position of the most intense line reflections ascribed to fcc Pt and different Pt-Sn alloy phases formed (fcc $Pt_{1-x}Sn_x$, Pt_3Sn and hcp PtSn).

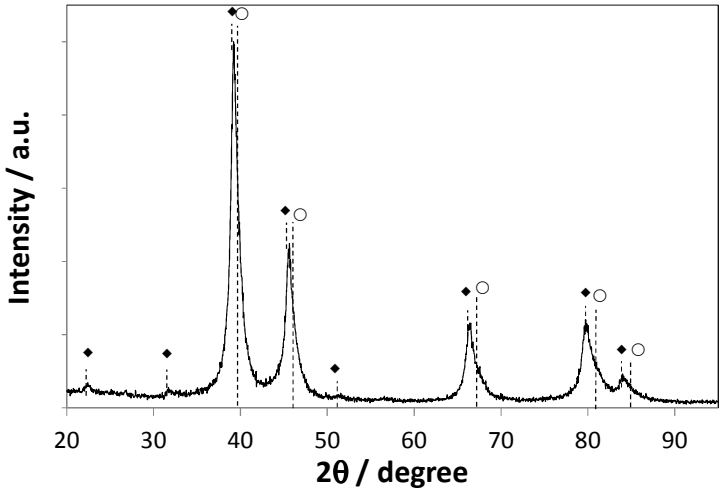

Fig. 1 X-ray diffraction pattern of 8.3SnPt/C-III-A sample. Diamond Pt_3Sn, Circle $Pt_{1-x}Sn_x$

The lattice parameter usually reported for fcc Pt is 3.917 Å [55]. Since the atomic radius of Sn is larger than that of Pt, an expansion of the unit cell according to Vegard's law should be expected. It is well known that upon formation of the PtSn solid solutions the incorporation of tin into the fcc structure of platinum results in shift of the peaks to lower 2θ values. As evidenced from the XRD patterns depicted in Fig. 2, upon tin incorporation not only peaks shifted to lower 2θ values (comparing to 2θ values the fcc structure of Pt (see Fig. 2A)), but a second set of peaks characteristic to the presence of a near-stoichiometric fcc Pt_3Sn phase (denoted as fcc Pt_3Sn in Table 2) appears. Furthermore, as illustrated in Figure 1, in Sn-modified samples characteristic superlattice reflections ascribed to the Pt_3Sn phase are also observed. The lattice parameter derived from the reflections of fcc Pt_3Sn phase could reflect the presence of a certain amount of the Pt-rich solid solution (denoted as fcc $Pt_{1-x}Sn_x$ in Table 2). The calculation of the lattice parameters can get an answer about tin and platinum atomic composition characteristic for the Pt-Sn alloy phases.

The XRD patterns of the samples with Pt/Sn ratio between 2.7 and 3.0 (see Figs. 2A, 2B and 2D and Table 2) reveal that $Pt_{1-x}Sn_x$ and a near-stoichiometric fcc Pt_3Sn are the only crystalline phases. In two samples with higher tin content (11.0SnPt/C-IV and 13.8SnPt/C-V) reflections assigned to the presence of small amount of hcp PtSn phase (see Fig. 2C and Table 2) were also observed. Reflections be assigned to Sn oxides were not found.

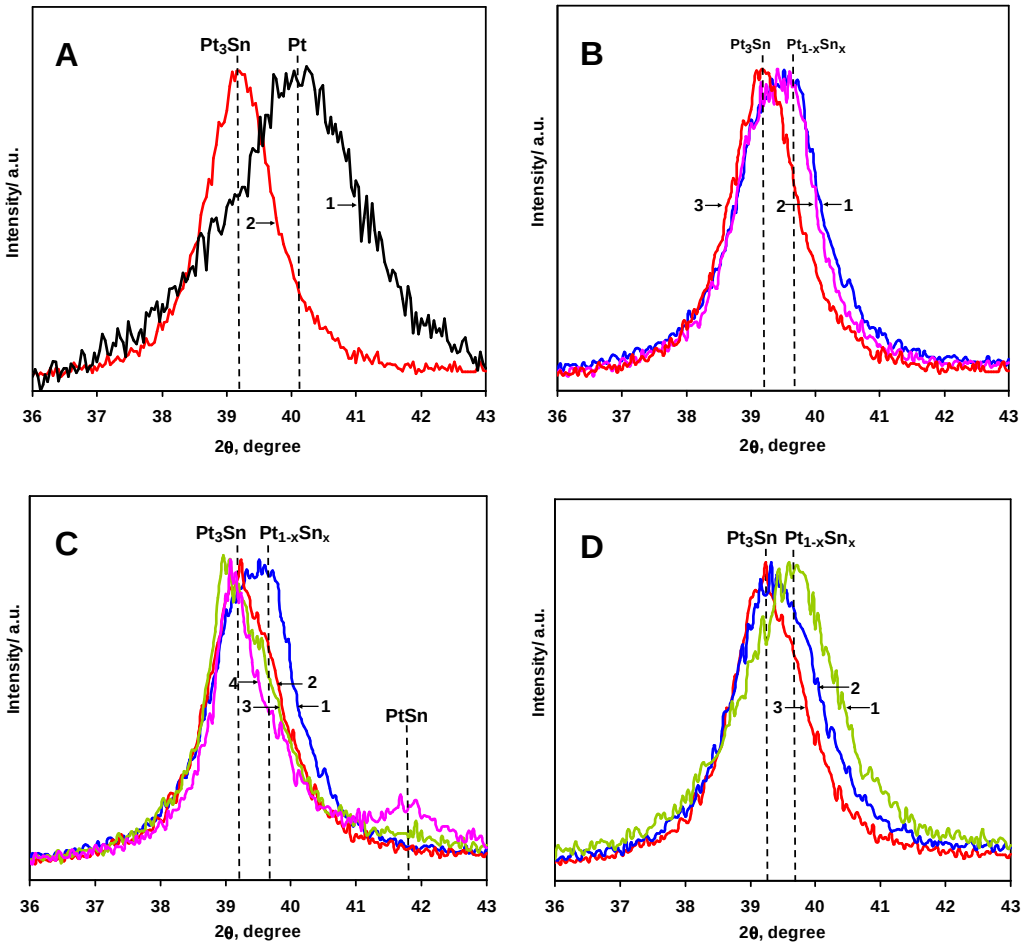

Fig. 2 X-ray diffraction pattern of parent Pt/C and SnPt/C catalysts. Influence of the preparation conditions on the position of the most intense reflections attributed to fcc Pt and different PtSn alloy phases (fcc $Pt_{1-x}Sn_x$, Pt_3Sn and hcp PtSn). **A** Influence of tin incorporation: Pt/C (1) and 8.3SnPt/C-III-A with the highest fcc Pt_3Sn content (2). **B** Influence of the preparation conditions of 8.3SnPt/C samples: 8.3SnPt/C-IV (1), 8.3SnPt/C-III-B (2) and 8.3SnPt/C-III-A (3). **C** Influence of the tin content: 8.3SnPt/C-IV (1), 9.1SnPt/C-III (2), 11.0SnPt/C-IV (3) and 13.8SnPt/C-V (4). **D** Influence of the temperature of H_2 pre-treatment of 9.1SnPt/C-III sample: without TPR (1), 250°C (2) and 350°C (3)

A careful deconvolution of XRD peaks allows calculation of the parameters of the Pt-rich ($Pt_{1-x}Sn_x$) and the Sn-rich phase (Pt_3Sn) lattices. The calculated values range between that of Pt (3.917 Å) and the pure intermetallic fcc Pt_3Sn phase (4.0015 Å) are summarized in Table 2. It can be seen that the lattice parameter of the Sn-modified samples is larger than that of Pt/C. This applies to both Pt_3Sn and $Pt_{1-x}Sn_x$ phases and it is in good agreement with the incorporation of Sn into the Pt lattice. Relative abundance of $Pt_{1-x}Sn_x$ and Pt_3Sn phases for all samples are also presented in Table 2.

For the catalysts with the desired Pt/Sn= 3.0 ratio and reduced in H_2 at 350°C the lattice parameter of the Sn-rich phase was a= 3.975 Å. As presented in Table 2 in these samples the crystalline phase consists of about 75 % Pt_3Sn and 25 % PtSn solid solution. Contrary to that

upon reduction of the catalyst with the same tin content (8.3SnPt/C-III-A) in H_2 at higher temperature (400°C) a near-stoichiometric fcc Pt_3Sn phase with lattice parameter a= 3.99 Å and relative abundance 85 % can be prepared. However, treatment at 400°C leads to an increase of the crystallite size (see Table 2). The influence of the T_{red} of 8.3SnPt/C samples on the X-ray diffraction pattern was demonstrated in Fig. 2B.

The increase of the lattice parameter for a near-stoichiometric Pt_3Sn phase up to a= 3.99 Å (see Table 2) was observed for the catalysts with higher tin content (Pt/Sn≤ 2.7). However, use of four and five consecutive tin anchoring periods results in the increase of the reaction time of step I and, as a consequence, in pronounced increase of the average crystallite size of the Sn-rich phase (see Fig. 2C and Table 2).

Deconvolution of XRD peaks also allows calculation of the lattice parameters of the Pt-rich phase ($Pt_{1-x}Sn_x$). As shown in Table 2 the lattice parameter for this phase is between 3.933 Å and 3.945 Å. The first value is close to lattice parameter of the $Pt_{90}Sn_{10}$ phase (whose lattice parameter is a=3.934 Å [56]). It can be proposed that higher values correspond to the PtSn solid solutions with higher Sn content in the Pt sublattice (10 at.% < Sn < 25 at.%). Relative abundance of Pt-rich phase varied from 15 and 35 %. As can be seen in Table 2 the dispersion of Pt-rich phase usually was slightly higher (or equal) than that one of Sn-rich phase.

The influence of the T_{red} on the content of crystalline phases was also included in Table 2. The XRD patterns (Fig. 2D) were recorded after H_2 pre-treatment of the 9.1SnPt/C-III sample at 250 and 350°C. Moreover the XRD analysis was also performed on this sample without additional high-temperature treatment (after the surface modification (step I) and before step II). As shown in Table 2 different pre-treatments have no influence on the lattice parameter values calculated for both crystalline phases. According to the phase analysis (see Table 2) after treatment at 250 and 350°C relative abundance of Pt_3Sn phase was slightly higher on sample treated at 350°C (80% vs. 75%). Nevertheless, the predominance of the $Pt_{1-x}Sn_x$ phase (75%) could be evidenced in the sample analyzed after step I (Fig. 2D). As emerges from the XRD results the increase of the average crystallite size of both Pt-Sn phases starts after the increase of the T_{red} from 250 up to 350°C.

TEM images of the blank Pt/C and Sn-modified samples along with the corresponding histograms displaying particle size distribution are depicted in Figs. 3 and 4. The TEM micrographs show the presence of spherical metallic particles supported on carbon particles. The mean size observed for Pt/C (see Fig. 3A) is 4.1 ± 1.6 nm. It is known that incorporation of tin results in an increase of the size of bimetallic particles. For the 8.3SnPt/C-IV sample

with the desired Pt/Sn= 2.9 ratio (Fig. 3B) only small increase of the mean particle sizes was observed (5.0 ± 1.9 nm).

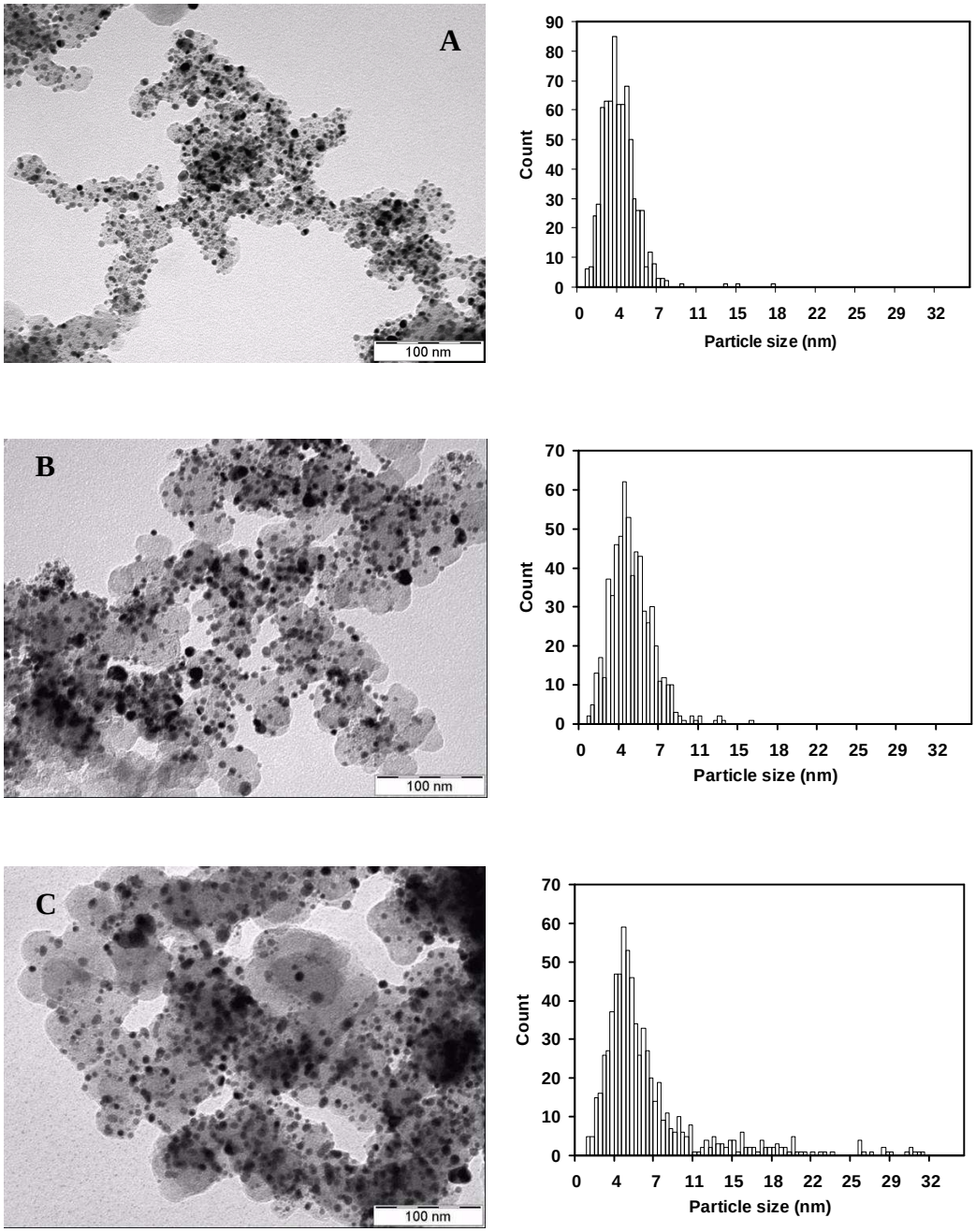

Fig. 3 TEM images and histogram of particle size distribution for **A** blank Pt/C, **B** 8.3SnPt/C-IV and **C** 8.3SnPt/C-III-A samples

From the low magnification micrographs a good dispersion of the metal particles on the carbon support in this sample is deduced. As emerges from the results there are certain discrepancies between the average crystallite size determined from XRD scans as well as the main particle size calculated from the histograms derived from TEM pictures. The former exceeds always the latter one. Actually, XRD, accounting for the long range periodicity in crystallites, is not sensitive to small particles (≤ 2.5 nm). As a consequence, in X-ray

diffraction patterns information originated from the larger crystallites dominates over that from the smaller one leading to an apparent shift to presence of larger crystallites.

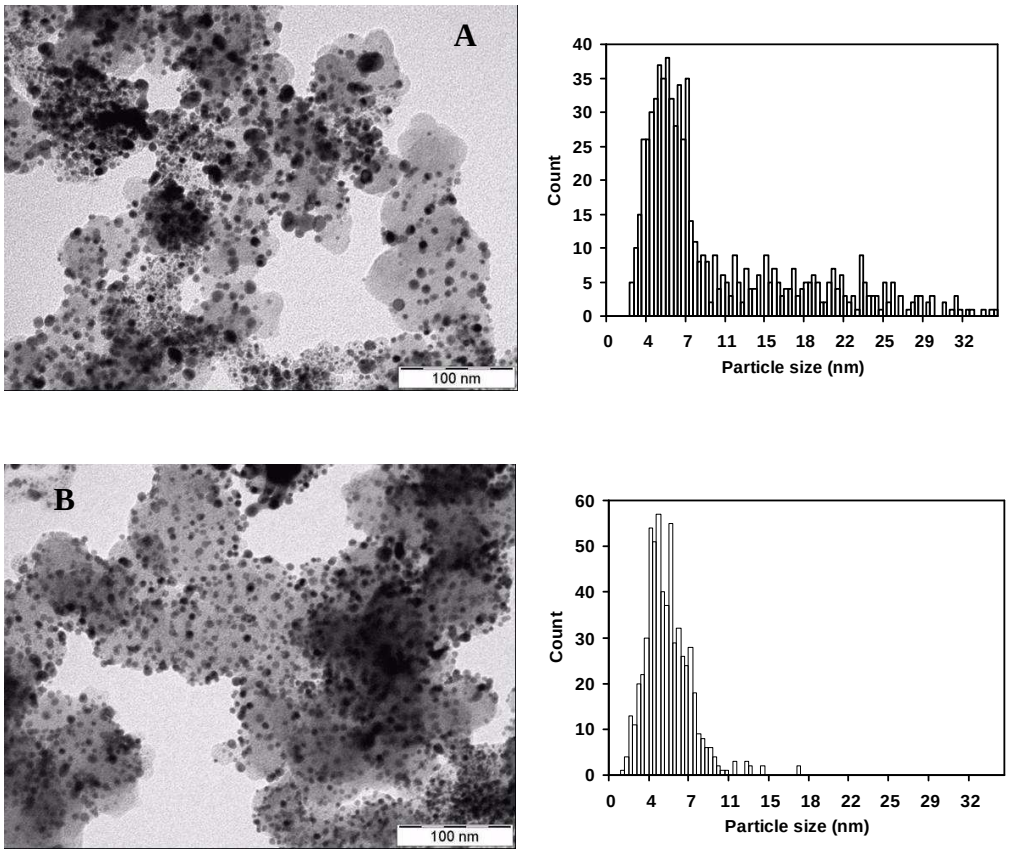

Fig. 4 Influence of the temperature of H_2 pre-treatment of 9.1SnPt/C-III sample at **A** 350°C and **B** 250°C on TEM images and histogram of particle size distribution

As shown in Table 2, upon increasing of both the T_{red} (up to 400°C) and the [$SnEt_4$] concentration ([$SnEt_4$]= 0.034 M) an increase of the Pt_3Sn phase lattice parameter and average particle size was observed. These data are in accordance with TEM results (Figs. 3C and 4A). Mean particle sizes are, 7.0 ± 5.1 nm and 10.6 ± 8.2 nm for 8.3SnPt/C-III-A and 9.1SnPt/C-III samples, respectively.

The influence of the T_{red} at 350°C and 250°C on the particle size was also demonstrated by TEM studies (Fig. 4A-B). As shown in Fig. 4B the treatment in H_2 at 250°C results in rather small particles with narrow size distribution (5.5 ± 2.1 nm). Taking into account that relative abundance of Pt_3Sn phase in both samples is quite similar, the use of the T_{red}= 250°C in step II can be recommended.

EDS analysis (images not shown) of different regions of the samples reveals that mean atomic Pt/Sn ratios were 2.86, 3.13 and 2.54 respectively for 8.3SnPt/C-IV, 8.3SnPt/C-III-A and 9.1SnPt/C-III sample treated in H_2 at 350°C. These data are in a good agreement with the Pt/Sn ratios presented for these catalysts in Table 1. Reduction of 9.1SnPt/C-III sample at

250°C resulted in slightly lower value of Pt/Sn= 2.44. These results correlate with our earlier studies [38,39], which demonstrate that complete reduction of SnO_x phase can be reached at $T_{red} \geq 300°C$.

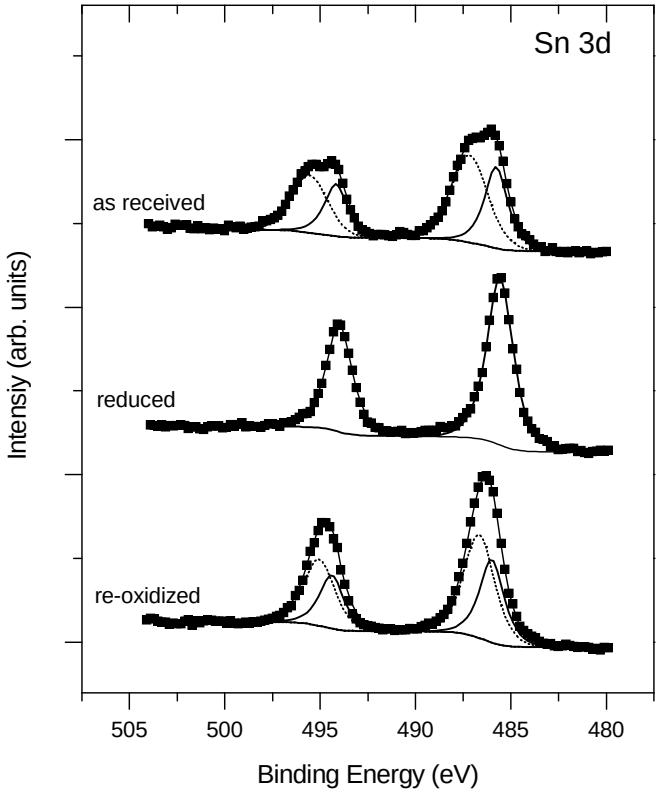

Fig. 5 Sn 3d core level spectra of 8.3SnPt/C-III-A sample in the "as received" state, after reduction at 350°C in H_2 and after re-oxidation. Fitting components due to metallic Sn and SnO_2 are also presented by means of *solid* and *dotted lines*, respectively

Standard deviation of the composition analyses was ca. 2-3 %, which means that relative abundance of Pt and Sn are homogeneous through the analyzed regions of the samples. The atomic composition of individual particles was also analyzed by EDS. These results show that compositional difference between big and small particles is not detectable. Furthermore no evidence of Sn segregation was found. In line with XRD results, no SnO_2 phases in the Sn-modified Pt/C samples were found by means of the EDS analysis.

The surface composition of catalysts was studied by XPS. Fig. 5 shows Sn 3d core level spectra of 8.3SnPt/C-III-A sample after different pre-treatments. Relevant compositional and chemical state data are presented in Table 3.

It is necessary to mention that samples were used in electrochemical tests in the "as received" form, so the characterization results of this state may be more relevant for the electrochemical properties. However, the study of the reduced form reflects on the real structure of the catalysts prepared by CSRs. As was mentioned above, all tin anchored onto the platinum is expected to be in Sn^0 state. As far as Pt-Sn alloy phases are easily oxidized [38], the contact of samples with air upon the storage results in oxidation of some part of tin.

"As received" reference Pt/C sample contains only carbon, oxygen and Pt. The Pt $4f_{7/2}$ binding energy of 71.5 eV corresponds well to the literature data of Pt^0. Nevertheless, the Pt 4f envelope is somewhat broad, which is either due to a small oxidized Pt component shifted towards higher binding energies from the metallic signal or due to the presence of very small nanoparticles, which is known to broaden the core level spectrum. Nonetheless, the oxygen content of the sample seems to be connected to carbon.

Table 3 Binding energies (eV) of Pt ($4f_{7/2}$) and Sn ($3d_{5/2}$) electrons

Sample	**Treatment**	**Pt $4f_{7/2}$ BE (eV)**	**Sn $3d_{5/2}$ BE (eV)**	**O 1s BE (eV)**	**Pt/C (at/at)**	**Sn/C (at/at)**	**O/Sn (at/at)**	**O/C (at/at)**	**Pt/Sn (at/at)**
Pt/C reference	as received	71.5	-	532.0 –OH, CO_x	0.044	-	-	0.055	-
8.3SnPt/C-III-A	as received	71.4	485.8 (25%) Sn^0	530.8 SnO_2	0.027	0.016	2.67	0.044	1.67
			486.7 (75%) Sn^{4+}	532.6 –OH, CO_x					
	H_2 treated	71.3	485.6 (100%) Sn^0	532.0 –OH, CO_x	0.031	0.011	0.5	0.005	3.0
	re-oxidized	71.5	485.9 (40%) Sn^0	530.9 SnO_2	0.028	0.017	3.67	0.061	1.67
			486.7 (60%) Sn^{4+}	532.6 –OH, CO_x					
8.3SnPt/C-IV	as received	71.4	485.8 (39%) Sn^0	531.0 SnO_2	0.028	0.017	3.33	0.055	1.67
			487.2 (61%) Sn^{4+}	532.6 –OH, CO_x					

The 8.3SnPt/C-III-A sample contains Pt in essentially the same form as that of the reference Pt/C sample, as judged from the shape and position of the Pt 4f envelope. As seen from Fig. 5 the Sn 3d core level structures contain two, strongly overlapping doublets, which can be separated by peak fitting. The more intense doublet with its $3d_{5/2}$ peak at 486.7 eV can be assigned to SnO_2. The other doublet with the $3d_{5/2}$ peak at 485.8 eV is very probably due to Sn^0, although this binding energy is somewhat high for bulk metallic Sn (484.6-485.2 eV for Sn $3d_{5/2}$ [46]) and may also correspond to SnO. The O 1s signal from the "as received" sample contains two contributions, one from SnO_2 and one from carbon-bonded oxygen species. The surface Pt/Sn atomic ratio 1.67 calculated from XPS spectrum is much lower in the "as received" state than the bulk Pt/Sn atomic ratios calculated from the material balance of tin anchoring (see Pt/Sn= 3.0 in Table 1) indicating the enrichment of Sn-oxide on the surface of the metallic particles and/or its presence also over the carbon support.

The behavior of the Sn 3d and O 1s core levels upon reduction (essentially unchanged BE for the Sn^0 component accompanied by the almost complete disappearance of oxygen) very strongly suggests that even the "as received" sample contains Sn in metallic state. The shift of the metallic Sn 3d signal towards higher binding energies can then be attributed to either size effects (as in small nanoparticles core levels tend to shift towards higher binding energies) or to formation of Sn-Pt alloy phases. Reduction effectively removes all SnO_2 related spectral features (see Fig. 5), while the Pt 4f core levels also become narrower, which might be attributed to reduction of PtO_2 or narrowing particle size. It is necessary to mention that SnO_x can be reduced to Sn^0 only in atomic contact with Pt [38,39,48]. Consequently, obtained results demonstrate the effectiveness of CSRs in the exclusive formation of Sn-Pt bimetallic nanoparticles along with suppression of tin-support interaction.

As a result of treatment in H_2, atomic ratios of O/C and Sn/C decreased (see Table 3). The decrease of the Sn/C atomic ratio could be the consequence of the diffusion of the metallic Sn over the metal particles into Pt or Sn-Pt alloy phase. The diffusion of tin would involve the increase of the Pt/C ratio. Indeed, upon reduction in H_2 at 350°C, Pt/C atomic ratio increased (see Table 3). The surface Pt/Sn atomic ratio (Pt/Sn= 3.0) became similar to the bulk ratio (see Table 1).

A one day air exposure of the sample results in the partial restoration of the SnO_2 content as evidenced by the Sn 3d and O 1s core levels (see Fig. 5 and Table 3). Nevertheless, the Sn^0 content remains higher than that was in the "as received" sample. In our previous study the enrichment of tin in the surface layers of the alloy-type Sn-Pt catalysts has been evidenced [38]. In the presence of O_2 and H_2 the reversible interconversion of $PtSn \leftrightarrow Sn^{4+} + Pt$ can easily proceeded even at room temperature and the surface character of the involved species was proposed.

The same chemical states as in "as received" 8.3SnPt/C-III-A sample were observed in 8.3SnPt/C-IV, while the proportion of metallic Sn was higher. As seen from data presented in Table 3 the proportion between Sn^0 and Sn^{4+} obtained over 8.3SnPt/C-IV and 8.3SnPt/C-III-A after one day air exposure (re-oxidized sample) is quite similar. However, taking into account that Sn-Pt alloy phases are easily oxidized, the observed difference can also be assigned to the prolongation of the contact of samples with air (or air storage conditions).

3.3 Electrooxidation of methanol and CO

CO oxidation on the Sn-modified Pt/C samples was evaluated by means of the CO-stripping technique. The voltammograms for the CO_{ad} oxidation on the parent Pt/C and the SnPt/C electrocatalysts are shown in Fig. 6A-C.

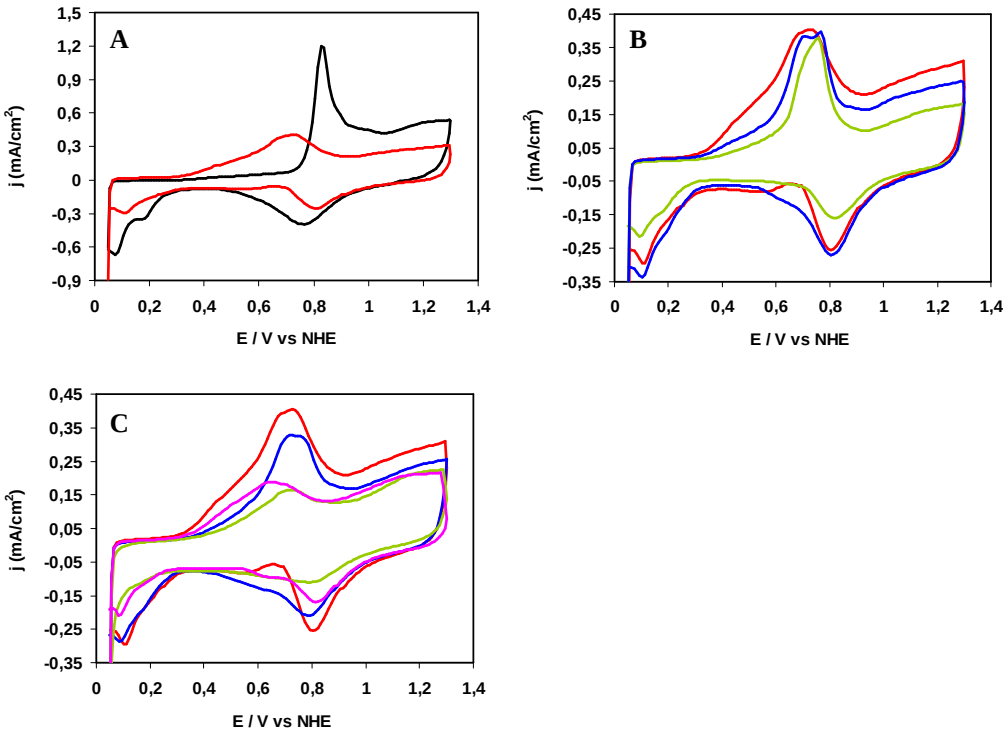

Fig. 6 CO oxidation (stripping analysis) on parent Pt/C and Sn-modified Pt/C catalysts. **A** Influence of tin: Pt/C (*black line*) and 8.3SnPt/C-IV (*red line*); **B** Influence of the preparation conditions of 8.3SnPt/C samples: 8.3SnPt/C-IV (*red line*), 8.3SnPt/C-III-A (*green line*) and 8.3SnPt/C-III-B (*blue line*); **C** Influence of the tin content: 8.3SnPt/C-IV (*red line*), 9.1SnPt/C-III (*blue line*), 11.0SnPt/C-IV (*green line*) and 13.8SnPt/C-V (*pink line*). Ag/AgCl and Pt was used as reference and counter electrodes, respectively. The electrolyte applied was 0.5 M H_2SO_4. Cyclic voltammograms were recorded by 10 $mV \cdot s^{-1}$ polarization rate. (For interpretation of the references to color in this figure legend, the reader is referred to the web version of the article)

The hydrogen oxidation peaks, usually appearing in the voltammograms of Pt-based catalyst between $0.0 < E < 0.4$ V, are not observed in the forward scan of voltammograms shown in Fig. 6. This feature is indicative of the full blocking of the catalysts surface due to the formation of Pt-CO_{ad}. Once CO_{ad} becomes oxidized (see the positive currents in the voltammograms) the peaks corresponding to formation of adsorbed hydrogen are clearly visible in the voltammograms, indicating the complete oxidation of CO_{ad}. In our previous [9] and other [11] studies the importance of the Pt_3Sn phase in the CO electrooxidation reaction was highlighted. It should be stated that on Pt_3Sn surfaces CO is adsorbed on the Pt sites rather than on Sn ones [57]. Remarkably, upon addition of tin the onset potential of CO oxidation has been shifted by 500 mV to less positive potentials, which indicates a significant

improvement in the CO oxidation ability of the Sn-modified samples in comparison to the Pt/C catalyst (see Fig. 6A).

Also, the shape of the oxidation peaks is rather different; CO_{ad} oxidation on Sn-modified Pt/C is a broad peak from ca. 200 to 800 mV, whereas a rather well defined peak is recorded for the CO_{ad} electrooxidation on Pt/C. It is well documented that CO oxidation on SnPt/C catalysts obeys a truly bifunctional mechanism in which CO is adsorbed on Pt whereas Sn sites nucleate OH_{ad} species at less positive potentials than Pt [58,59]. It should be recalled that CO electrooxidation on Pt-based electrodes takes place in the presence of OH_{ad} species which become nucleated on Pt/C in acid medium at E > 0.6 V but they are available on the surface of Sn-containing electrodes at potentials as low as 100 mV.

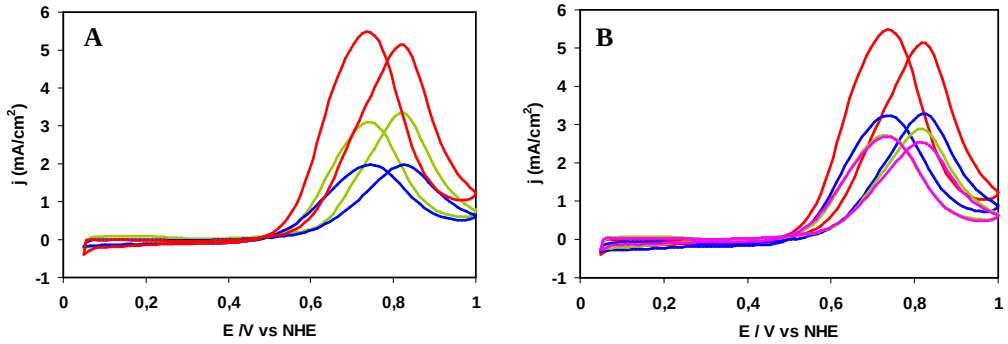

Fig. 7 Methanol electrooxidation on Sn-modified Pt/C catalysts. **A** Influence of the preparation conditions of 8.3SnPt/C samples: 8.3SnPt/C-IV (*red line*), 8.3SnPt/C-III-A (*green line*) and 8.3SnPt/C-III-B (*blue line*); **B** Influence of the tin content: 8.3SnPt/C-IV (*red line*), 9.1SnPt/C-III (*blue line*), 11.0SnPt/C-IV (*green line*) and 13.8SnPt/C-V (*pink line*). Ag/AgCl and Pt was used as reference and counter electrodes, respectively. The electrolyte applied was 0.5 M H_2SO_4 and 1 M methanol. Cyclic voltammograms were recorded by 10 $mV \cdot s^{-1}$ polarization rate. (For interpretation of the references to color in this figure legend, the reader is referred to the web version of the article)

As shown in Fig. 6B at low potentials the current density increases upon increasing of the number of consecutive anchoring periods. Obviously, application of more anchoring periods also means that the desired amount of $SnEt_4$ has to be added in smaller concentration per one period. The most active catalyst (8.3SnPt/C-IV) was prepared using the lowest [$SnEt_4$] concentration in this series of experiments and four consecutive tin anchoring periods (line 1 in Table 1). Two other catalysts with desired Pt/Sn= 3 were pre-treated in H_2 at various temperatures (350°C vs. 400°C). The current density of 8.3SnPt/C-III-B was higher than that recorded with the sample with the highest fcc Pt_3Sn content (8.3SnPt/C-III-A). Increased particle size observed on 8.3SnPt/C-III-A sample after reduction at 400°C (Fig. 3B and Table 2) can be a reason of its lower activity in the CO_{ad} oxidation. These results demonstrate the importance to find an optimum for the T_{red} applied in step II. While, according to our previous

results, Pt_3Sn alloy is advantageous, the higher particles size may lead to smaller activity in electrooxidation reaction. Consequently, these two phenomena might have an opposite effect on the electrocatalytic activity. According to Fig. 6C the decrease of the current density was observed upon an increase of the tin content comparing to desired Pt/Sn= 3.

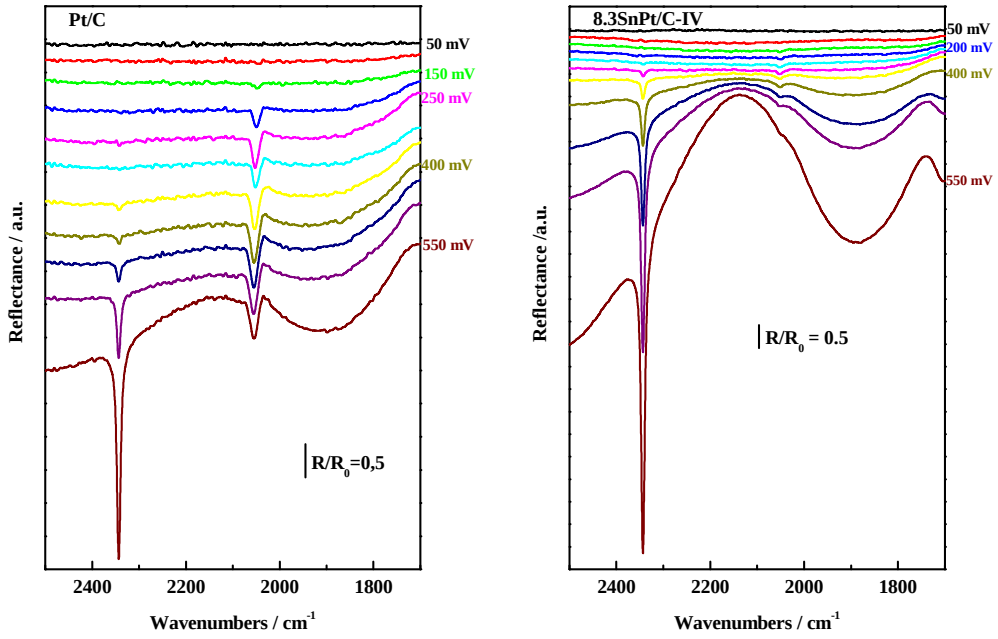

Fig. 8 EC-FTIR spectra of recorded during CH_3OH electrooxidation on Pt/C and 8.3SnPt/C-IV in 0.1 M $HClO_4$ electrolyte. The spectra were recorded at 50 mV intervals and normalized to the spectrum recorded at 50 mV (R_0)

Nonetheless, a strong promotion of the CO oxidation process is observed on all prepared catalysts when compared to Pt/C. This result is in good agreement with previous discussion in the sense that CO oxidation on SnPt/C samples is promoted due to the formation of Sn-OH_{ad} species.

The voltammograms of methanol electrooxidation on all studied Sn-modified Pt/C catalysts are presented in Fig. 7A-B. Fig. 7A shows that for the preparation of SnPt/C electrocatalysts with desired Pt/Sn= 3 ratio, the use of low [$SnEt_4$] concentration and four consecutive tin anchoring periods can be recommended.

As emerges from Fig. 7B the performance of the catalyst is negatively influenced by increasing the Sn content in the catalyst and in the alloy. Based on this result it can be concluded that the performance of fcc Pt_3Sn phase is superior to that of the hcp PtSn phase for both CO and methanol oxidation reactions in terms of current density. According to the most accepted mechanism for the methanol electrooxidation reaction, three neighbouring Pt sites

are necessary for methanol adsorption-dehydrogenation reaction and the possibility to find such Pt ensembles decreases with the decreasing Pt/Sn ratio.

The performance of Pt/C and 8.3SnPt/C-IV for the electrooxidation of CO_{ad} and methanol has been evaluated by electrochemical techniques along with in situ techniques such as EC-IRAS. Representative FTIR spectra (not shown) of the oxidation of CO_{ad} with Pt/C and 8.3SnPt/C-IV were collected at 50 mV intervals in 0.1 M $HClO_4$. Both set of spectra show a band at 2343 cm^{-1} indicative of the formation of CO_2. Also, a band at 2057 and 2065 cm^{-1} is observed in the spectra of Pt/C and 8.3SnPt/C-IV, respectively and ascribed to linearly bounded CO on Pt sites. As deduced from the spectra, the onset of CO_{ad} oxidation, i.e. the appearance of the CO_2 band, shifts to lower potentials in the Sn-modified electrode (200 mV) as compared to that one in Pt/C (350 mV), in good agreement with the voltammetry results. These values are in line with previous reports for CO_{ad} electrooxidation on Pt/C and SnPt/C catalysts [41], and confirm that Sn is a good promoter for the oxidation of CO_{ad} on Pt-based catalysts. The FTIR spectra recorded during the electrooxidation of methanol in 0.1 M $HClO_4$ are shown in Fig. 8. In line with previous results, methanol is efficiently oxidized to CO_2 on both electrocatalysts as deduced from the observation of a band at 2343 cm^{-1} ascribed to the formation of CO_2 band. However, the actual performance of the electrocatalysts is noticeably different. For instance, the onset for CO_2 production is 250 mV on 8.3SnPt/C-IV but it shifts by 100 mV to higher potentials on Pt/C. Not only does 8.3SnPt/C-IV promote the complete oxidation of methanol at lower potentials than Pt/C. More importantly, a careful inspection of the spectra reveals that the actual reaction pathway is different in both catalysts. Thus, a band at 2054 cm^{-1} is clearly observed in the set of spectra recorded during methanol oxidation on Pt/C. This band, which can be observed in the spectra recorded at potentials as low as 150 mV, is indicative of the formation of CO_{ad} species during the oxidation of methanol, probably resulting from the dehydrogenative adsorption of methanol on Pt sites. The formation of CO_{ad} species on 8.3SnPt/C-IV can be also appreciated in the spectra shown in Fig. 8. However, the intensity of the band is significantly lower than that on the Pt/C electrocatalyst indicating that the formation of CO_{ad} is suppressed in the Sn-modified catalysts. This observation also indicates that the direct oxidation pathway is the favored pathway in the Sn-containing catalysts. This observation can be rationalized by taking into account that ensembles of at least three vicinal Pt atoms are necessary for CO formation during methanol oxidation as clearly shown by Cuesta [60]. It appears that the diluting effect of Sn in the Pt network results in a lower number of ensembles containing tree contiguous Pt atoms and hence to a lower

formation of CO and as a consequence to a promotion of the non-CO pathway for the oxidation on methanol.

4 Conclusions

Optimum experimental conditions were found for the controlled synthesis of SnPt/C electrocatalysts with Pt/Sn= 1.8-3.0 ratios and exclusive Sn-Pt interaction. As demonstrated by XRD the incorporation of Sn onto Pt/C was achieved satisfactorily yielding a near-stoichiometric fcc Pt_3Sn alloy phase along with a certain amount of the $Pt_{(1-x)}Sn_x$ solid solution. No evidence of the presence of SnO_2 phases were found by means of the XRD and EDS analysis. The content and dispersion of the fcc Pt_3Sn phase depends on (i) the amount and concentration of $SnEt_4$, (ii) the number of consecutive tin anchoring periods and (iii) final T_{red} applied in step II. According to in situ XPS studies H_2 pre-treatment at 350°C resulted in complete reduction of tin to Sn^0. These results demonstrate effectiveness of CSRs in the exclusive formation of Sn-Pt bimetallic nanoparticles.

The performance of the intermetallic SnPt/C catalysts in the CO and methanol electrooxidation reactions depends on Pt/Sn ratio, content of fcc Pt_3Sn alloy phase and the size of bimetallic particles. It was demonstrated that decrease of the [$SnEt_4$] concentration added per one period, accompanied with an increase of the number of consecutive anchoring period, resulted in an increase of the activity in both reactions. Remarkably, tin has a strong dilution effect of the platinum sites decreasing the number of Pt ensembles necessary for the methanol dehydrogenation to CO. As a consequence, the direct oxidation of methanol to CO_2 is promoted in the Sn-modified electrodes.

Acknowledgments This study was performed under the joint Hungarian- Spanish research project HAS-CSIC/2009-2010 (№ 3). The authors are grateful to the Hungarian Scientific Research Fund (OTKA, Grant №: K100793) for financial support. Sergio Rojas acknowledges financial support from the Spanish Ministry of Science and Innovation through project ENE-15381. The authors thank Prof. J.L. Margitfalvi for the interest and helpful discussion of this work.

References

1. Antolini E, Gonzalez ER (2011) Catal Today 160:28-38

2. Antolini E (2007) J Power Sources 170:1-12

3. Martínez-Huerta MV, Rodríguez JL, Tsiouvaras N, Peña MA, Fierro JLG, Pastor E (2008) Chem Mater 20:4249-4259

4. Martínez-Huerta MV, Rojas S, Gómez de la Fuente JL, Terreros P, Peña MA, Fierro JLG (2006) Appl Catal B: Environmental 69:75-84

5. Liu CW, Chang YW, Wei YC, Wang KW (2011) Electrochim Acta 56:2574-2581

6. Colmati F, Antolini E, Gonzalez ER (2006) J Power Sources 157:98-103
7. Profeti LPR, Simoes FC, Olivi P, Kokoh KB, Coutanceau C, Léger JM, Lamy C (2006) J Power Sources 158:1195-1201
8. Min M, Cho J, Cho K, Kim H, (2000) Electrochim Acta 45:4211-4217
9. García-Rodríguez S, Somodi F, Borbáth I, Margitfalvi JL, Peña MA, Fierro JLG, Rojas S (2009) Appl Catal B: Environmental 91:83-91
10. García-Rodríguez S, Peña MA, Fierro JLG, Rojas S (2010) J Power Sources 195:5564-5572
11. Arenz M, Stamenkovic V, Blizanac BB, Mayrhofer KJ, Markovic NM, Ross PN (2005) J Catal 232:402-410
12. Stamenkovic VR, Arenz M, Lucas CA, Gallagher ME, Ross PN, Markovic NM (2003) J Am Chem Soc 125:2736-2745
13. Higuchi E, Miyata K, Takase T, Inoue H (2011) J Power Sources 196:1730-1737
14. Xiong L, Manthiram A (2005) Electrochim Acta 50:2323-2329
15. Siné G, Fóti G, Comninellis Ch (2006) J Electroanal Chem 595:115-124
16. Li L, Huang M, Liu J, Guo Y (2011) J Power Sources 196:1090-1096
17. García-Rodríguez S, Rojas S, Peña MA, Fierro JLG, Baranton S, Léger JM (2011) Appl Catal B: Environmental 106:520- 528
18. Lamy C, Rousseau S, Belgsir EM, Coutanceau C, Léger JM (2004) Electrochim Acta 49:3901-3908
19. Léger JM, Rousseau S, Coutanceau C, Hahn F, Lamy C (2005) Electrochim Acta 50:5118-5125
20. Bönnemann H, Britz P, Vogel W (1998) Langmuir 14:6654-6657
21. Zhou WJ, Song SQ, Li WZ, Zhou ZH, Sun GQ, Xin Q, Douvartzides S, Tsiakaras P (2005) J. Power Sources 140 :50-58
22. Song SQ, Zhou WJ, Zhou ZH, Jiang LH, Sun GQ, Xin Q, Leontidis V, Kontou S, Tsiakaras P (2005) Int J Hydrogen Energy 30:995-1001
23. Zhou W, Zhou Z, Song S, Li W, Sun G, Tsiakaras P, Xin Q (2003) Appl Catal B: Environmental 46:273-285
24. Jiang L, Sun G, Sun S, Liu J, Tang S, Li H, Zhou B, Xin Q (2005) Electrochim Acta 50:5384-5389
25. Jiang L, Colmenares L, Jusys Z, Sun GQ, Behm RJ (2007) Electrochim Acta 53:377-389
26. Baranova EA, Amir T, Mercier PHJ, Patarachao B, Wang D, Page YL (2010) J Appl Electrochem 40:1767-1777
27. Colmenares L, Wang H, Jusys Z, Jiang L, Yan S, Sun GQ, Behm RJ (2006) Electrochim Acta 52:221-233
28. Liu Z, Guo B, Hong L, Lim TH (2006) Electrochem Commun 8:83-90
29. Kim JH, Choi SM, Nam SH, Seo MH, Choi SH, Kim WB (2008) Appl Catal B: Environmental 82:89-102
30. Colmati F, Antolini E, Gonzalez ER (2007) Appl Catal B: Environmental 73:106-115
31. Colmati F, Antolini E, Gonzalez ER (2005) Electrochim Acta 50:5496-5503
32. De Souza RFB, Parreira LS, Silva JCM, Simoes FC, Calegaro ML, Giz MJ, Camara GA, Neto AO, Santos MC (2011) Int J Hydrogen Energy 36:11519-11527
33. Simoes FC, dos Anjos DM, Vigier F, Léger JM, Hahn F, Coutanceau C, Gonzalez ER, Tremiliosi-Filho G, de Andrade AR, Olivi P, Kokoh KB (2007) J Power Sources 167:1-10
34. De Souza RFB, Parreira LS, Rascio DC, Silva JCM, Teixeira-Neto E, Calegaro ML, Spinace EV, Neto AO, Santos MC (2010) J Power Sources 195:1589-1593
35. Somodi F, Peng Z, Getsoian AB, Bell AT, (2011) J Phys Chem C 115:19084-19090
36. Margitfalvi JL, Borbáth I, Tompos A (1998) Catal Today 43:29-41

37. Margitfalvi JL, Borbáth I, Hegedűs M, Tompos A (2002) Appl Catal A: General 229:35-49
38. Margitfalvi JL, Borbáth I, Lázár K, Tfirst E, Szegedi Á, Hegedűs M, Gőbölös S (2001) J Catal 203:94-103
39. Margitfalvi JL, Borbáth I, Hegedűs M, Tfirst E, Gőbölös S, Lázár K (2000) J Catal 196:200-204
40. Margitfalvi JL, Borbáth I, Hegedűs M, Gőbölös S (2001) Appl Catal A: General 219:171-182
41. Herranz T, García S, Martínez-Huerta MV, Peña MA, Fierro JLG, Somodi F, Borbáth I, Majrik K, Tompos A, Rojas S (2012) Int J Hydrogen Energy 37:7109-7118
42. Crabb EM, Marshall R, Thompsett D (2000) J Electrochem Soc 147:4440-4447
43. Fairley N (2006) http://www.casaxps.com
44. Mohai M (2004) Surf Interface Anal 36:828–832
45. Mohai M (2003) XPS MultiQuant: Multi-model X-ray photoelectron spectroscopy quantification program, Version 3.00.16 http://www.chemres.hu/aki/XMQpages/XMQhome.htm
46. Wagner CD, Naumkin AV, Kraut-Vass A, Allison JW, Powell CJ, Rumble Jr JR (2003) NIST X-ray Photoelectron Spectroscopy Database, Version 3.4, National Institute of Standards and Technology, Gaithersburg, MD, http://srdata.nist.gov/xps/
47. Moulder JF, Stickle WF, Sobol PE, Bomben KD (1992) Handbook of X-ray Photoelectron Spectroscopy, Perkin-Elmer Corp Eden Prairie, Minnesota, USA
48. Bocanegra SA, de Miguel SR, Borbath I, Margitfalvi JL, Scelza OA (2009) J Mol Catal A: Chemical 301:52-60
49. Coloma E, Sepúlveda-Escribano A, Fierro JLG, Rodriguez-Reinoso F (1997) Appl Catal A: General 150:165-183
50. Coloma E, Sepúlveda-Escribano A, Fierro JLG, Rodriguez-Reinoso F (1994) Langmuir 10:750-755
51. Torres GC, Jablonski EL, Baronetti GT, Castro AA, de Miguel SR, Scelza OA, Blanco MD, Peña-Jiménez MA, Fierro JLG (1997) Appl Catal A: General 161:213-226
52. van Dam HE, van Bekkum H (1991) J Catal 131:335-349
53. de Miguel SR, Roman-Martinez MC, Jablonski EL, Fierro JLG, Cazorla-Amoros D, Scelza OA (1999) J Catal 184:514-525
54. Paál Z, Wootsch A, Teschner D, Lázár K, Sajó IE, Györffy N, Weinberg G, Knop-Gericke A, Schlögl R (2011) Appl Catal A: General 391:377-385
55. Durussel P, Massara R, Feschotte P (1994) J Alloy Compounds 215:175-179
56. Radmilovic V, Richardson TJ, Chen SJ, Ross Jr PN (2005) J Catal 232:199-209
57. Stamenković V, Arenz M, Blizanac BB, Mayrhofer KJJ, Marković NM, Ross PN (2005) Surface Science 576:145-157
58. Liu P, Logadottir A, Norskov JK (2003) Electrochim Acta 48:3737-3742
59. Koper MTK (2004) Surf Sci 548:1-3
60. Cuesta A (2006) J Am Chem Soc 128:13332-13333